BioChem

MDPI

Article

Enhancement and Characterization of the Accelerated Clearing of *Bacillus thuringiensis* by Phage 0524phi7-1

Meagan S. Phillips [1,†], Maria Rojero [1,†], Theo Courteaux [2], James P. Chambers [2] and Philip Serwer [1,*]

[1] Department of Biochemistry and Structural Biology, UT Health, San Antonio, TX 78229, USA; weaverrosen@uthscsa.edu (M.S.P.); rojero@uthscsa.edu (M.R.)
[2] Department of Molecular Microbiology and Immunology, The University of Texas at San Antonio, San Antonio, TX 78249, USA; theo.courteaux@utsa.edu (T.C.); james.chambers@utsa.edu (J.P.C.)
* Correspondence: serwer@uthscsa.edu; Tel.: +1-210-567-3765
† These authors contributed equally to this work.

Abstract

Background/Objectives: Viruses are universally found not to have programmed motility functions (propulsion). However, plaque assays of phage 0524phi7-1, an aggregating phage, sometimes generate accelerated bacterial lysis spreading seen via asymmetric, semi-turbid and clear zones in plaque-supporting agarose gels. The semi-turbid zones subsequently clear and expand, without producing phage-resistant bacteria. This apparent phage propulsion could be useful (e.g., for phage therapy of bacterial diseases) if enhanced and better understood. **Methods/Results**: Here, we found random initiation of semi-turbid zones that were derived from miniature satellite-plaques in numbers too high to reliably count. Previous considerations suggest non-participation of bacterial motors. The known possibilities to explain apparent phage propulsion include diffusiophoresis, driven by concentration gradients between agarose gel fibers, and Marangoni force, derived from surface tension gradients along agarose gel fibers. We found that 1.1% Tween 80, a non-ionic detergent, (1) had no visible effect on either a bacterial lawn or circular plaques, (2) accelerated lysis spreading and (3) drove phage aggregates toward edges of cleared zones, as observed by light microscopy. Electron microscopy demonstrated phage aggregation via lateral tail–tail associations. **Conclusions**: A working, data-consistent hypothesis is that accelerated lysis spreading is caused by Marangoni force acceleration of monomeric and aggregated phages and phage aggregate exclusion from (previously demonstrated) bacterial clumps.

Keywords: bacteriophage aggregation; diffusiophoresis; Marangoni effect; non-ionic detergent; powered phage motion; surface tension

Check for updates

Academic Editors: Manuel Aureliano and Buyong Ma

Received: 5 August 2026
Revised: 15 October 2026
Accepted: 19 October 2026
Published: 22 October 2026

Copyright: © 2026 by the authors. Licensee MDPI, Basel, Switzerland. This article is an open access article distributed under the terms and conditions of the Creative Commons Attribution (CC BY) license.

1. Introduction

Phage 0524phi7-1 displays four unusual and relatively aggressive, anti-bacterial behaviors during plaque assays. The first is the formation of asymmetric, semi-turbid and clear zones that are much larger than circular plaques. The semi-turbid zones completely clear during a second overnight incubation. The second is the formation of miniature, possibly satellite-plaques in only limited regions of a Petri plate during plaque assays. Not-yet-visible satellite-plaques are proposed to cause the semi-turbid zones [1]. Parenthetically, satellite-plaques are not the same as satellite-phages. Satellite-phages are, behaviorally, genetic parasites (not satellites) of the main phage [2,3]. Phages from satellite-plaques, when cloned, produce a distribution of plaques that is not significantly different from the distribution of plaques of the original phage [4].

Third, after they clear, both semi-turbid zones and circular plaques continue to enlarge for days, which is a behavior not usually associated with the first two when it (occasionally) exists in other phages. The fourth unusual behavior is the phage's bypass of the emergence of phage-resistant bacteria [1], a behavior not, to our knowledge, reported for other phages.

Phage 0524phi7-1 is a myophage with a tail 210 nm long, a head about 91 nm in diameter, and a 157.103 Kb genome: family, *Herelleviridae*; genus, *tsarbombavirus*. This phage also undergoes aggregation far beyond that of most other studied phages [1]. The cause is not known for the accelerated, asymmetrically directed phage migration (enhanced phage propulsion) that drives the formation of larger-than-a-plaque zones of lysis. The data indicate that the host bacteria cannot move through the gels used here and that, therefore, the origin is not ride-hitching on the host [1]. This latter conclusion is supported by the non-motility of the host for a phage T4 mutant that exhibits similar accelerated phage-induced lysis spreading [4].

In the current study, we initially perform tests to determine the pattern of formation of asymmetric, larger-than-a-plaque lysis zones during a conventional plaque assay. Next, we perform tests to develop possibilities for enhancing and understanding the apparent enhanced phage propulsion. We obtain data that reveal that the non-ionic detergent, Tween 80, enhances apparent propulsion. This raises the possibility that propulsion arises from at-surface forces derived from the inhomogeneity of surface tension (Marangoni effect/force) along gel-forming fibers (in-gel Marangoni effect hypothesis). We use this as a working hypothesis to help explain our (unusual) data and to find ways to use these data to accelerate the spreading of bacterial lysis. The Marangoni force, in general, drives particles in the direction of low to high surface tension [5–8].

2. Materials and Methods

Generative artificial intelligence was not used anywhere in this manuscript.

2.1. Plaque Assay and Purification of Bacteriophages

The initial isolation of phage 0524phi7-1 and its subsequent preparative, in-gel propagation in a Petri plate (plate stock) are described in [1]. All subsequent propagation was from the original stock. Here, the growth medium in both the lower-layer and the upper-layer gels was the same as in [1]: 10 g tryptone and 5 g KCl in 1 L of water with 0.001 M sterilized $CaCl_2$ added after autoclaving (T broth). The pH of the T-broth was adjusted to 6.0 with HCl. The lower-layer gel was 1.0% Bacto agar (Fisher Scientific, Waltham, MA, USA). The upper-layer gel was 0.4% Seakem Gold agarose (Lonza, Rockland, ME, USA).

Infectivity assays were done with the following procedure. The host (~60 µL of an overnight culture) and phages were added to 3.0 mL molten agarose at 50 °C in T-broth. This mixture was immediately poured onto the bottom agar and allowed to gel at room temperature. The Petri plate was incubated at 30 °C. Multiple platings of phages from one diluted phage preparation were performed by repeating this procedure during a time span of less than 0.5 min per Petri plate with two investigators independently working and using a single temperature-controlled block for molten plating solutions. Phage 0524phi7-1 was diluted less than 1.0 h. before plating. The upper-layer agarose gel was firm and had no visible region of surface fluid in any Petri plate. Phage T4 [4] was plated with the same procedure, except that a 0.4% agar plaque-supporting gel was used. Phage T3 and the related phage, phiII [1], were plated with the procedure used for T4, except that the concentration of the plaque-supporting gel was raised to 0.8% because of the larger-than-T4 and -0524phi7-1 size of the T3 and phiII plaques.

Phage 0524phi7-1 was partially purified by (1) low-extent centrifugation to remove bacteria and large bacterial fragments, followed by (2) higher-extent centrifugation to pellet

the phage and remove relatively small contaminants, and, finally, (3) rate-zonal centrifugation in a 10–35% sucrose gradient pre-poured above a layer of 62% sucrose (details: [1]). Two preparations of phage 0524phi7-1 were used here. The same sucrose gradient fraction (phage aggregate-containing) was used for the phages from both preparations (fraction indicated in Figure 4 of [1]).

In the sample used for plating, the total mature-length phage DNA component was quantified by (1) expelling phage DNA from capsids; (2) fractionating the DNA by gel electrophoresis, as in [1]; and (3) quantifying the mature phage DNA band. The quantification was performed by comparing the fluorescence of this band to the fluorescence of phage T3 DNA bands that had a DNA amount known from measuring the optical density at 260 nm. We could not perform the same optical density measurement for fractionated phage 0524phi7-1 because of the presence in phage aggregates of capsids that had sub-genomic-length DNA [1]. From plaque assays that did not have semi-turbid zones, the ratio of plaque-forming units to the number of mature-length DNA molecules was 0.93 ± 0.20, not significantly different from 1.0. Based on this observation, phages diluted for plating were not detectably aggregated when plated. All experiments had no-phage-inoculum-control plates, which never had plaques.

2.2. Imaging of Petri Plates

Images of the Petri plates were captured with an iPhone 16 camera (Apple Inc., Cupertino, CA, USA). When indicated, the image was pre-magnified on the stage of a New Brunswick Scientific C110 plaque counter (New Brunswick Scientific Co., Inc., Edison, NJ, USA).

2.3. Light Microscopy

For light microscopy, the indicated region of the upper-layer gel of a plaque assay was (1) excised with a sterile spatula and (2) placed between a cover glass and a glass microscope slide. The specimen was flattened by pressing on the cover glass with the rubber eraser attached to a pencil.

The specimen was visualized by use of an Olympus BX60 fluorescence microscope (upright) (Olympus Corporation, Tokyo, Japan) in phase contrast mode. Real-time video of the microscope images was recorded with a sensitive analog CCD camera (EXvision, SuperCircuits, Austin, TX, USA) connected to a VHS recorder (Panasonic AG-1980; Panasonic Corporation, Osaka, Japan). The images were projected via a cathode ray tube (VM-1205B, ProVideo, Austin, TX, USA) and photographed with an iPhone 16 camera (Apple, Inc., Cupertino, CA, USA). Scan lines were digitally removed by blurring in Microsoft PowerPoint (Redmond, WA, USA).

2.4. Electron Microscopy

To prepare plaque contents for electron microscopy, a 2–4 mm segment of plaque-supporting agarose gel was excised with a sterile spatula and fixed by submersion in 4.0% formaldehyde, 1.0% glutaraldehyde, 0.11 M sodium phosphate, pH 7.3. After fixation for at least 2.0 h. at room temperature, the gel was (1) washed for 5 min in 1.5 mL of 0.1 M sodium phosphate, pH 7.3, and (2) post-fixed for 30 min, at room temperature, in 1.0% osmium tetroxide dissolved in Zetterqvist's buffer [9].

A fixed, plaque-supporting agarose gel was then (1) dehydrated, (2) embedded in Epon 812 resin and (3) thin-sectioned by the use of procedures previously described [10]. A Leica EM UC6 microtome (Leica Microsystems, Nussloch, Germany) was used to cut thin sections; the speed of cutting was varied as indicated in Section 3.5. The sections were stained with 7% uranyl acetate for 30 s, followed by Reynold's lead citrate for 20 s in a microwave oven (0.035 W cm^{-3}) [10].

Electron microscopy was performed with a JEOL JEM-1400 electron microscope (JEOL Ltd., Tokyo, Japan). Images were recorded with an AMT image capture engine, version: 7 (Advanced Microscopy Techniques, Corp. (AMT), Woburn, MA, USA).

3. Results

3.1. Patterns of Semi-Turbid Zone Formation

To investigate patterns of semi-turbid zone initiation, a plaque assay was repeated 40 times. The various repetitions all used the same procedure and the same materials. All 40 were performed within a 15 min interval. After a 20.0 h co-incubation, nine Petri plates had only circular plaques; 31 Petri plates had both circular plaques and 1–5 extended, sometimes separate, sometimes merged, asymmetric, larger-than-a-plaque semi-turbid zones like either the small or the large zones in Figure 1a–c, which shows images of three of these latter Petri plates. The largest semi-turbid zones (arrows in Figure 1a–c) had (1) sub-regions with clear plaques that had both size smaller and a density higher than those of plaques outside of the semi-turbid zone. The relatively high density of the small plaques indicated that most, and possibly all, of them were satellite-plaques that had been started by phage migration from a previously established plaque. The alternative of most small-plaque generation via phage aggregate dissociation was eliminated via the large number of small plaques and the high specific infectivity of the inoculum (Section 2.1). Smaller semi-turbid zones (arrowheads in Figure 1) presumably were initiated later.

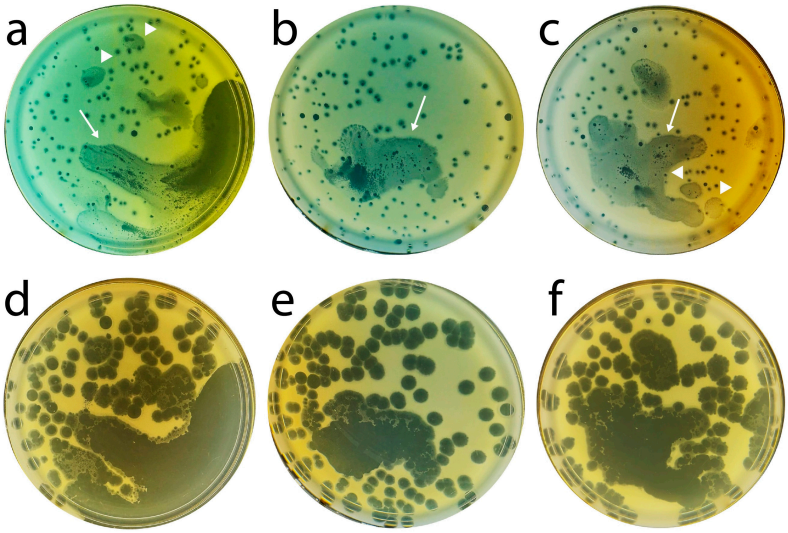


Figure 1. Conventional plaque assay of phage 0524phi7-1. Three (of 40) assays are shown after incubation for (**a**–**c**) 20.0 h. and (**d**–**f**) 44.0 h. The Petri plates in (**a**–**c**) are the same as those in (**d**–**f**), respectively. Arrows: large semi-turbid zones; arrowheads: small semi-turbid zones.

After 24.0 additional hr. of incubation, all semi-turbid zones completely cleared and expanded while keeping the original shape of the semi-turbid zone (Figure 1d–f for the Petri plates in Figure 1a–c, respectively). Also, during the second incubation, (1) no new semi-turbid zones were generated in any Petri plate, and (2) no miniature satellite-plaques remained unmerged.

In Figure 1a–c, based on geometrical approximations of the area of cleared zones, the total area of one of the larger semi-turbid zones is usually 20–100× the surface coverage of circular plaques and will be made higher in Section 3.4. Surface coverage is defined as the total area of circular plaques that are not in a semi-turbid zone, but exist in a region with an area the same as the area of a semi-turbid zone. This is seen in one Petri plate. Thus, something is accelerating the spread of infectious phages in the semi-turbid zones during

the first 20.0 h. incubation. This acceleration occurs asymmetrically, as seen in the shape of the semi-turbid zones. The asymmetry of phage spread is also seen in most of the smaller semi-turbid zones (arrowheads in Figure 1a–c).

The phages in the semi-turbid zones are still infective for the bacteria in these zones, as seen via the clearing of the asymmetric, semi-turbid zones in Figure 1d–f. This clearing suggests that the number of satellite-plaques was higher than immediately apparent in Figure 1a–c.

3.2. Additional Satellite-Plaques

This latter conclusion was confirmed when we, by chance, caught the development of a semi-turbid zone at an appropriate point, as shown in Figure 2. Figure 2 has a relatively large semi-turbid zone in the lower part of the Petri plate, accompanied by a smaller semi-turbid zone above it. The key point is that the large semi-turbid zone in Figure 2 has miniature satellite-plaques in numbers too high to reliably count (over 10,000). These were seen at any plaque size compatible with the resolution of the image. The entire large semi-turbid zone subsequently cleared completely. Clearing is beginning at the right in Figure 2.

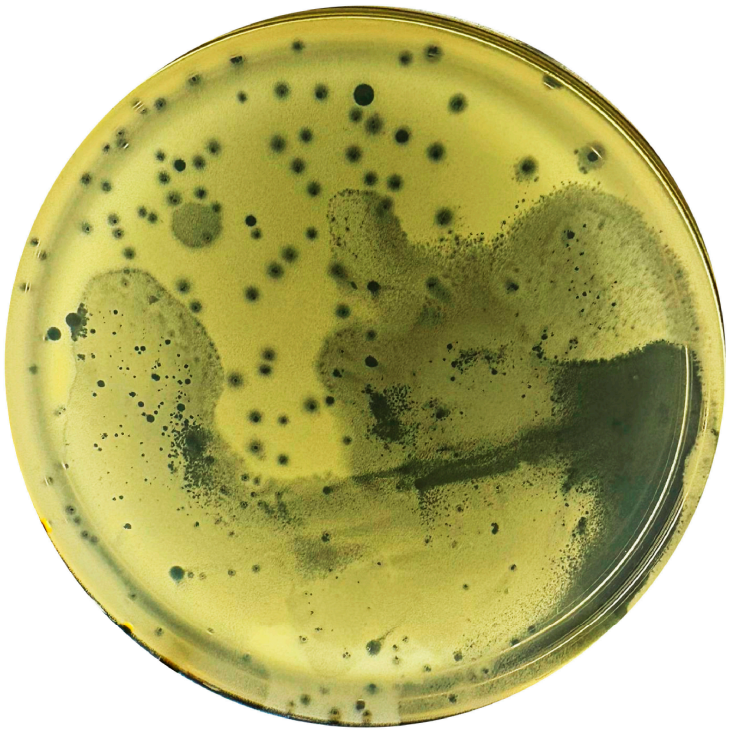


Figure 2. Satellite-plaques in a relatively large semi-turbid zone that has started to clear after incubation for 20.0 h.

Satellite-plaques in a semi-turbid zone were initiated by phages migrating non-randomly. Random phage migration would have produced a semi-turbid zone and a clear successor that were circular in outline.

3.3. The Effects of Adding Detergent

To further discriminate possible mechanisms, we added the surface-tension-lowering [11], non-ionic detergent, Tween 80, to the upper- and lower-layer gels during plating. After overnight incubation, this addition did not have a visible effect on either bacterial propagation or circular phage plaque formation at Tween 80 concentrations of 0.5–3.0%. Thus, given the effect of Tween 80 on surface tension, a finding of no effect on larger-than-

circular plaque zones would have been a strong indicator that the in-gel Marangoni effect hypothesis is not correct.

The result was that 0.5–1.1% Tween 80 visibly enhanced the formation, average surface area and clearing of semi-turbid zones after incubation for 19.5 h. This was initially observed for five plates each, with 0.5, 0.7, 0.9, and 1.1% Tween 80, when compared to 5 control plates without Tween 80. Examples of plates with 1.1% Tween 80 are in Figure 3a–c. The control plates all had at least 3x lower average coverage by semi-turbid zones and lower amounts of clearing within semi-turbid zones. The effect of adding 1.1% Tween 80 was confirmed in a separate experiment, with 20 plates each, of a control and Tween 80. Thus, the in-gel Marangoni effect hypothesis was not rejected and, as discussed in Sections 4.1 and 4.2, was consistent with a reasonable rendition of additional details.

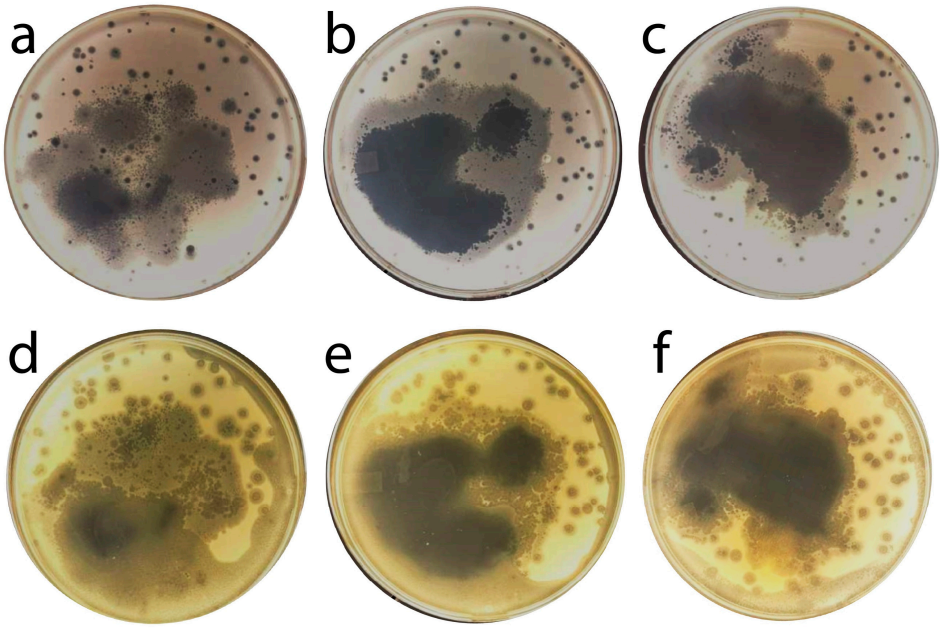


Figure 3. Effect of uniform 1.1% Tween 80 on plaque formation. (**a**–**c**) 19.5 h. incubation; (**d**–**f**) 43.5 h incubation.

Tween 80 did not have this effect on the plating of several non- or low-aggregating phages, including wild-type coliphages T3, T4 and phiII (10 Petri plates tested for each phage). Phage 0524phi7-1 has at least one new feature, possibly a tendency to aggregate, that is required for the acceleration of host clearing.

When the experiment of Figure 3 was continued (total time = 43.5 h.), the control plates underwent the changes previously seen in Figure 1d–f. However, Petri plates with the 0.5, 0.7, 0.9, and 1.1% Tween 80 were different in the following ways. Unlike the controls, (1) most significantly, the partially cleared semi-turbid zones either did not undergo shape-preserving expansion or underwent much less shape-preserving expansion; (2) in either case, these zones did not complete internal clearing and became more cloudy at the periphery of previously clear regions (Figure 3d–f; same Petri plates as in Figure 3a–c); and (3) shape-changing semi-turbid zone expansion occurred, as most easily seen at the bottom of the Petri plates in Figure 3d–f. None of these three outcomes has ever been seen in over 100 trials without the addition of Tween 80. The clouding of the periphery of previously clear regions, without evidence of phage-resistant bacteria, suggested the accumulation of phage aggregates in these regions.

In preliminary experiments, we tested the non-ionic detergent Brij 35 instead of Tween 80. However, Brij 35 disrupted the propagation of the host at concentrations of 0.7% or 0.9% (10 Petri plates tested at each concentration of Brij 35).

3.4. Light Microscopy

We tested for the presence of phage aggregates by use of phase contrast microscopy of excised regions of the upper-layer gel of plaque assays with Tween 80 added. We used plaque assays like the one in Figure 3, except that the bottom-layer gel did not have Tween 80 (1.1% Tween 80 in the top layer only). This resulted in a more concentrated region of semi-turbidity at the edge of completely cleared zones (Figure 4a) that expanded for a time longer than in Figure 3: two days. We do not know the reason for the difference.

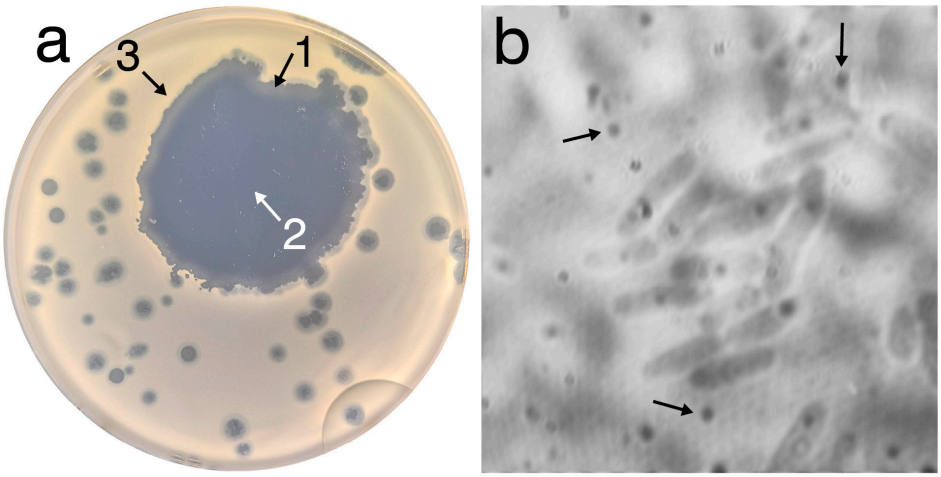


Figure 4. Light microscopy of zones of accelerated clearing stimulated by Tween 80. (**a**) Image of Petri plate after 48.0 h. of incubation. Arrows indicate regions examined by light microscopy. (**b**) Light microscopy of region indicated by arrow #1 in (**a**).

We excised a sample from the semi-turbid ring (sample location, arrow #1 in Figure 4a) and observed it directly by phase contrast light microscopy. We also observed material from the clear interior (sample location, arrow #2) and clear zone-proximal surrounding bacterial lawn (sample location, arrow #3). This was one of five identical plates, four of which had a zone of clearing comparable to the one in Figure 4a. Of five control plates, all had only circular plaques; none had a zone of accelerated bacterial lysis.

The results of the light microscopy were the following. First, images of the clear interior (arrow #2 in Figure 4a) had nothing visible. Second, the turbid ring (arrow #1 in Figure 4a) had bacteria or cytoplasm-deficient bacterial "ghosts" and a new, smaller particle (smaller than spores) that was often indistinguishable from a sphere (arrows in Figure 4b). These smaller particles were possibly phage aggregates; they were too large and refractive to be single phage particles. These smaller particles were similarly present in a clear zone-proximal bacterial lawn (arrow #3 in Figure 4a), but not in a bacterial lawn that was not close to a clear zone like the one in Figure 4a.

In a separate experiment, these smaller particles were found to be at an even higher (>10×) density in the clear region within 1–2 mm of the turbid edge. These particles were associated with the advancing front of the clear region. This continued to be the case as this front further advanced.

The experiment of Figure 4a was repeated with Tweens 20, 40 and 60. The result was not significantly different (two independent sets of five Petri plates each tested for each Tween type).

3.5. Electron Microscopy

To further characterize the smaller particles of the previous section, we performed electron microscopy of thin sections of the sample at the turbid-edge region of Figure 4a.

The result was that phage aggregates were observed. Aggregation occurred via tails that were aligned primarily side to side (Figure 5a–d). The aggregates were usually distal from other structures except for the fibers of the agarose gel; one of these fibers is indicated by an arrow in Figure 5a. An aggregate with six tails and two empty heads showing is in Figure 5a. Heads may have been attached to the other tails but not included in the thin section. Of 15 randomly selected aggregates, all had the same organization, except for variation in the number of heads and tails.

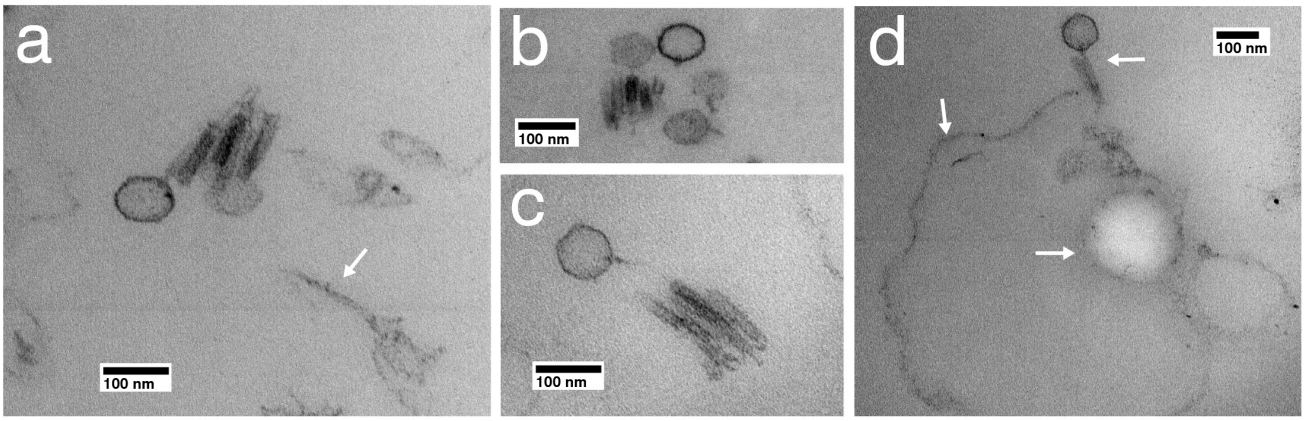


Figure 5. (**a**–**d**) Electron microscopy of phage aggregates in the sample indicated by arrow #1 in Figure 4a. Arrows: (**a**) a fiber of agarose gel; (**d**) top arrow, phage aggregate; middle arrow, bacterial membrane; bottom arrow, blank region that was possibly generated by scooping out a phage aggregate during thin sectioning.

The aggregates were accompanied by two other particles: (1) heads that were not visibly attached to anything else and (2) membranes of lysed cells, not visibly associated with a cell wall. These membranes were flexible, without uniform shape and devoid of visible content. In association with a two-phage aggregate (top arrow in Figure 5d), an example of a cell-wall-detached cellular membrane is indicated by the middle-left arrow in Figure 5d. These membranes (1) were usually not attached to phage aggregates and (2) were the dominant particles in the specimen. Host vesicles of the approximate size of phage aggregates were not observed.

All 15 of the above randomly selected aggregates had more tails than heads and some heads were empty. In addition, no aggregates of any type were observed when the speed of thin sectioning was raised from the 0.1 mm/sec used in Figure 5 to 0.6 mm/sec. The same embedded specimen was used. Apparently, the knife did not cut through aggregates as consistently at the higher speed. An occasional blank (presumably scooped out) region at 0.1 mm/sec (lowest arrow in Figure 5d) appears to be an example of this effect at the lower cutting speed.

4. Discussion

Phage 0524phi7-1 is not alone in its "sometimes" generation of asymmetric, satellite-plaque-accompanied zones of apparent phage propulsion. For example, phage T4 has been evolved to generate such zones that, after 18 h., are clearer and more asymmetric than those of phage 0524phi7-1 shown here ($T4_{Ar}$). As in the case of phage 0524phi7-1, other areas of the same $T4_{Ar}$ Petri plate have circular T4 plaques [4]. The data obtained here indicate random (stochastic) initiation of these zones. Whatever the details of this initiation, the finding of it for two different phages suggests the hypothesis that it is an adaptation that is selected during phage evolution in the wild and, therefore, has a function in the wild.

The clarity of the circular plaques of both phage 0524phi7-1 and phage $T4_{Ar}$ implies that a circular plaque does not include a peripheral zone of partial lysis, generated by lysis inhibition [12–14] for either phage. Therefore, the asymmetric zones of lysis seen here are, as they appear to be, characterized by the accelerated spread of phage infection. The accelerated spread of phage infection is not, like plaque asymmetry [13], something that can be generated by lysis inhibition. The non-participation of lysis inhibition in accelerated lysis spreading is supported by the fact that the circular plaques of $T4_{Ar}$ have the size and clarity of rapid lysis mutants, i.e., mutants that do not undergo lysis inhibition [13,14]. Thus, the following alternative explanation for the asymmetric zones appears to be excluded. These zones are the product of reaction-diffusion (which generates only circular plaques [15]) and lysis inhibition [13]. Apparently, phages 0524phi7-1 and $T4_{Ar}$ have a feature, possibly a tendency to aggregate, that accelerates the spread of lysis and that other well-studied phages do not manifest. Although a not-yet-considered (unknown to us), non-lysis inhibition-based biological mechanism is possible, a physical mechanism is favored for accelerated lysis spreading.

Independently of the mechanism, the detergent-induced increase in accelerated lysis spreading has potential use in the spreading of the phage therapy of surface bacterial infections. As the conditions required are learned, we will also learn whether/how this effect can be so used.

4.1. Relevant Considerations for Understanding Apparent Accelerated Phage Propulsion

The following observations are best explained by the dependence on phage aggregation of zones of accelerated lysis spreading and apparent accelerated phage propulsion. First, wild-type phage 0524phi7-1 aggregates more extensively than other wild-type phages [1]. Phage 0524phi7-1 also appears to be unique among current wild-type phages in its formation of these zones. Thus, phage aggregation and these zones occur in correlation. Second, in Sections 3.4 and 3.5, phage aggregates were found to be associated with the leading edge of zones of Tween 80-accelerated bacterial lawn clearing. Third, as described in Section 4.2 below, a possible mechanism for this correlation exists.

Diffusion (thermal motion)-driven phage migration is not the primary source of apparent accelerated phage propulsion. A sufficient reason is that the domination of semi-turbid zone spreading by diffusion-driven phage motion is inconsistent with the asymmetry of the semi-turbid zones. The asymmetry of these zones implies the guidance of phage motion to make satellite-plaque initiation directional. Perhaps not as obvious is that this guidance implies that phage thermal motion is small relative to motion caused by energy input from a force of some kind, probably chemically or physically derived. The theoretical reason is the second law of thermodynamics [16]. Empirically, this requirement for energy input was demonstrated, in the case of bacterial chemotaxis, by placing microscopic funnels in paths of the bacteria during chemotaxis. The bacteria were sterically concentrated by the funnels. When the bacteria were not undergoing chemotaxis, the funnels did not concentrate the non-motile bacteria even though the non-motile bacteria were undergoing thermal motion [17,18].

The proposed (not proven) mechanism for asymmetry-generating phage guidance, independent of the source of the required energy input, is the following. (1) Inhomogeneities in the plaque-supporting agarose gel occur during gelation. (2) These inhomogeneities generate funnel-like or funnel-equivalent structures of gel-forming fibers. (3) These structures guide phage motion. This mechanism is supported by the parallel, but separate, highly asymmetric zones of accelerated lysis sometimes seen for $T4_{Ar}$ (e.g., Figure 1 in [4]). Guided, energy-requiring motion is, for biology-based studies of phages, a concept that is typically not considered (e.g., [19]).

The phage propulsion mechanism is confirmed here to include the proliferation of satellite-plaques. In the absence of additional data, two additional aspects can explain the turbidity from cells between satellite-plaques in a semi-turbid zone: (1) the non-infection of these cells, and (2) infection without lysis, e.g., lysis inhibition [12–14], which might also have been evolutionarily selected, in part, to facilitate the infection-escape of some bacteria. The above considerations favor the first explanation. Lysogeny is not a possibility because phage 0524phi7-1 does not have genes for lysogeny [1].

4.2. The Force Involved

Assuming a physically derived source of most apparent accelerated propulsion, the stimulatory activity of a non-ionic detergent (surface-active) favors a force that originates at surfaces, rather than a force that originates at a distance from surfaces. In more detail, in the absence of fluid flow, surface-distal physical forces are comprehensively described by the thermodynamics of non-equilibrium systems. Translating from equations [20] to concrete physical concepts [21,22], two physical effects are involved: (1) the osmotic movement of water up concentration gradients (i.e., composite concentration gradients of all solutes released [23] by plaque-associated, lysed bacteria), some local to the particle being moved (i.e., within the Debye–Hückel-discovered double layer), and (2) electrophoretic particle motion induced by charge separations generated by difference in the diffusion constants of gradient-forming molecules (collectively called diffusiophoresis).

The first diffusiophoresis effect will drive particles up a concentration gradient [21,22]. Thus, it does not qualify to be the dominant effect seen here because the phages move away from previously initiated plaques. In the case of the diffusiophoresis of bacteria, the second effect is insensitive to the addition of non-ionic detergent [24], in contrast to the observation made here (Figures 3 and 4) in the case of phages. This observation suggests a minor role for diffusiophoresis, at most, and, via the elimination of alternatives, supports a major role for a surface-generated force.

Thus, we ask whether an in-plaque Marangoni effect hypothesis can explain our observations. The Marangoni effect drives particles along surfaces in the direction of low to high surface tension [6–8]. In the absence of added detergent, the expected direction is away from a plaque, along plaque-supporting gel fibers. The reason for this expectation is that the in-plaque surface tension will be lowered relative to the surroundings by proteins released [23] from lysed bacterial cells. The expected direction is the observed direction. Thus, an in-plaque Marangoni effect hypothesis is a plausible explanation.

Concerning the explanation of the effects of adding Tween 80, we begin with the following additional characteristics of the system involved. The overnight lawn in the plaque-supporting gel used here has most bacteria in multi-micron, tightly packed clumps that are separated by even larger spaces [25].

Along the agarose gel fibers in bacterial clumps, the average concentration of Tween 80 will be less than it is between the bacterial clumps. The reason is the substitution of bacteria for the Tween 80 solution. This will raise the surface tension differential between (1) bacterial clumps, which are relatively Tween 80-poor with relatively high surface tension along gel fibers, and (2) regions with either no bacteria or phage-lysed bacteria, which are relatively Tween 80-rich with relatively low surface tension. The result would be the detergent-enhanced driving of monomeric and aggregated phages along gel fibers toward uninfected bacterial clumps.

The effect of phage aggregation is reasonably represented by the following. The Marangoni force is found to be linearly proportional to the surface tension gradient and the particle size [5–8]. In solution, the resistance to motion is inversely proportional to the particle size, linearly if the particle is a sphere, which we will assume. If so, in the absence

of additional retardation via either a sieving or a binding effect, the net motion would not depend on the particle size. The sieving of an agarose gel would slow phage aggregates more than monomeric phages.

However, during collision with a bacterial clump, the larger a phage aggregate is, for steric reasons, the less likely the aggregate would be to penetrate the clump. In addition, even aggregated phages at a bacterial clump surface would be inhibited from infecting bacteria by the tail–tail contact seen in Figure 5. Thus, the larger an aggregate is, the higher the probability that the aggregate bypasses bacterial clumps, thereby increasing the probability that some bacterial clumps will be (temporarily) uninfected. Monomeric phages would have a high probability of infecting bacteria adjacent to the growing plaque and would, therefore, be depleted at the leading plaque edge.

Additional outcomes would be the observed driving of phage aggregates to the leading edge of a semi-turbid, subsequently cleared zone (Figures 4 and 5), (2) the formation of satellite-plaques when a phage aggregate does, at a low frequency, infect a bacterial clump (Figure 2) and (3) the eventual inhibition of lysis spreading by aggregates too large to migrate through the plaque-supporting gel (Figure 3d–f).

Finally, we note that, in the case of viruses for eukaryotes, hyper-virus spreading can occur via forces generated at a cell membrane without translational movement of the cell generating the force (surfing or actin-driven exit) [26–28]. Bacteria (1) have surfaces that are not known to engage in similar activity, to our knowledge, and (2) have rigid cell walls that would appear to prevent similar activity.

Thus, an in-gel Marangoni effect hypothesis provides a useful and empirically supported foundation for understanding the effects observed. This hypothesis does not currently have details of dynamics, such as the dynamics of particles moving along gel fibers in the presence of a known surface tension gradient. A direct, real-time analysis of the single-particle dynamics of this type is an objective for the future and will further test the hypothesis.

4.3. Limitation of Interpretation and Some Historical Points

In conclusion, we note that Marangoni force-propelled macroscopic motion was historically used to determine the boundaries of monolayers, a key aspect of the original determination of the existence of and size of atoms and molecules [29]. More recent work has quantified this force [5,6], and shown that it can occur (1) on the surface of agar gels [7] and (2) during the gelation of collagen [8]. In contrast, our data suggest that the Marangoni force also exists inside gels. We are not aware of a physics-based study in this latter area and assume that the quantitative details, beyond the approximate details presented here, will involve characteristics of the surfaces involved, e.g., gel fibers [30]. The previous non-observance of the effects introduced here is likely a result of the investigator rejection (with limited exception; [31,32]) of either phages that extensively aggregate or the conditions in which phages aggregate.

A detailed interpretation of our data is most limited by the absence of a characterizable system in which the inter-cell phage movements can be observed directly, by light microscopy, for example. Obtaining this system is an objective for the future.

Author Contributions: Conceptualization, M.S.P., M.R., J.P.C. and P.S.; methodology, M.S.P., M.R. and T.C.; validation, M.S.P., M.R., T.C., J.P.C. and P.S.; formal analysis, P.S.; investigation, M.S.P., T.C. and M.R.; resources, J.P.C. and P.S.; data curation, M.S.P. and M.R.; writing—original draft preparation, P.S.; writing—review and editing, M.S.P., M.R. and P.S.; visualization, M.S.P., M.R. and T.C.; supervision, P.S.; project administration, J.P.C. and P.S.; funding acquisition, J.P.C. and P.S. All authors have read and agreed to the published version of the manuscript.

Funding: This research was funded by the US National Science Foundation (STTR: 2409676) and the San Antonio Medical Foundation (2024).

Institutional Review Board Statement: Not applicable.

Informed Consent Statement: Not applicable.

Data Availability Statement: The data presented in this study are all available within one or more of the following: The figures and the text. The sequence of phage 0524phi7-1 is in GenBank: accession number PV296012.

Acknowledgments: The authors thank William Tolhurst for comments on the content of this manuscript and Barbara Hunter for performing the thin-sectioning for Figure 5. The authors have reviewed and edited the output and take full responsibility for the content of this publication.

Conflicts of Interest: P.S., M.S.P., M.R., and J.P.C. have an affiliation with the company Phage Refinery (www.phagerefinery.com). This company may make use of the results of this and future related studies. The funders had no role in the design of the study; in the collection, analyses, or interpretation of data; in the writing of the manuscript; or in the decision to publish the results.

References

1. Rojero, M.; Weaver-Rosen, M.; Serwer, P. Bypassing evolution of bacterial resistance to phages: The example of hyper-aggressive phage 0524phi7-1. *Int. J. Mol. Sci.* **2025**, *26*, 2914. [CrossRef] [PubMed]
2. Penadés, J.R.; Seed, K.D.; Chen, J.; Bikard, D.; Rocha, E.P.C. Genetics, ecology and evolution of phage satellites. *Nat. Rev. Microbiol.* **2025**, *23*, 410–422. [CrossRef] [PubMed]
3. Christie, G.E.; Calendar, R. Bacteriophage P2. *Bacteriophage* **2016**, *6*, e1145782. [CrossRef] [PubMed]
4. Rojero, M.; Weaver-Rosen, M.; Serwer, P. Reply to Abedon, S.T. Dual-receptor recognition, lysis inhibition, endolysin release, and reaction–diffusion as alternative explanations. comment on "Rojero et al. Bypassing evolution of bacterial resistance to phages: The example of hyper-aggressive phage 0524phi7-1. *Int. J. Mol. Sci.* **2025**, *26*, 2914". *Int. J. Mol. Sci.* **2025**, *26*, 11468. [CrossRef] [PubMed]
5. Ebrahimi, A.; Kazemzadeh, Y.; Akbari, A. Impact of the Marangoni phenomenon on the different enhanced oil recovery methods. *Heliyon* **2024**, *10*, e39919. [CrossRef] [PubMed]
6. Liu, H.; Deng, J. Influence of Marangoni effect on heat and mass transfer during evaporation of sessile microdroplets. *Micromachines* **2022**, *13*, 1968. [CrossRef] [PubMed]
7. Nonomura, Y.; Chida, S.; Seino, E.; Mayama, H. Anomalous spreading with Marangoni flow on agar gel surfaces. *Langmuir* **2012**, *28*, 3799–3806. [CrossRef] [PubMed]
8. Nerger, B.A.; Brun, P.T.; Nelson, C.M. Marangoni flows drive the alignment of fibrillar cell-laden hydrogels. *Sci. Adv.* **2020**, *6*, eaaz7748. [CrossRef] [PubMed]
9. Glauert, A. *Fixation, Dehydration and Embedding of Biological Specimens*; North-Holland Publishing Co.: New York, NY, USA, 1975.
10. Serwer, P.; Hunter, B.; Wright, E.T. Electron microscopy of in-plaque phage T3 assembly: Proposed analogs of neurodegenerative disease triggers. *Pharmaceuticals* **2020**, *13*, 18. [CrossRef] [PubMed]
11. Milanović, J.; Krstonošić, V.; Dokić, L. Insight into the interaction between carbopol® 940 and ionic/nonionic surfactant. *J. Dispers. Sci. Technol.* **2015**, *36*, 964–972. [CrossRef]
12. Abedon, S.T. Look who's talking: T-even phage lysis inhibition, the granddaddy of virus-virus intercellular communication research. *Viruses* **2019**, *11*, 951. [CrossRef] [PubMed]
13. Abedon, S.T. Dual-receptor recognition, lysis inhibition, endolysin release, and reaction–diffusion as alternative explanations. Comment on Rojero et al. Bypassing evolution of bacterial resistance to phages: The example of hyper-aggressive phage 0524phi7-1. *Int. J. Mol. Sci.* **2025**, *26*, 2914. *Int. J. Mol. Sci.* **2025**, *26*, 11368. [CrossRef] [PubMed]
14. Hvid, U.; Mitarai, N. Competitive advantages of T-even phage lysis inhibition in response to secondary infection. *PLoS Comput. Biol.* **2024**, *20*, e1012242. [CrossRef] [PubMed]
15. Yin, J.; McCaskill, J.S. Replication of viruses in a growing plaque: A reaction-diffusion model. *Biophys. J.* **1992**, *61*, 1540–1549. [CrossRef] [PubMed]
16. Fermi, E. *Thermodynamics*; Dover Publications: New York, NY, USA, 1956.
17. Galajda, P.; Keymer, J.; Chaikin, P.; Austin, R. A wall of funnels concentrates swimming bacteria. *J. Bacteriol.* **2007**, *189*, 8704–8707. [CrossRef] [PubMed]
18. Wan, M.B.; Olson Reichhardt, C.J.; Nussinov, Z.; Reichhardt, C. Rectification of swimming bacteria and self-driven particle systems by arrays of asymmetric barriers. *Phys. Rev. Lett.* **2008**, *101*, 018102. [CrossRef] [PubMed]

19. Lohrmann, C.; Holm, C.; Datta, S.S. Influence of bacterial swimming and hydrodynamics on attachment of phages. *Soft Matter* **2024**, *20*, 4795–4805. [CrossRef] [PubMed]
20. Annunziata, O. Diffusiophoresis of macromolecules within the framework of multicomponent diffusion. *Molecules* **2024**, *29*, 1367. [CrossRef] [PubMed]
21. Akdeniz, B.; Wood, J.A.; Lammertink, R.G.H. Diffusiophoresis and diffusio-osmosis into a dead-end channel: Role of the concentration-dependence of zeta potential. *Langmuir* **2023**, *39*, 2322–2332. [CrossRef] [PubMed]
22. Ganguly, A.; Alessio, B.M.; Gupta, A. Diffusiophoresis: A novel transport mechanism—Fundamentals, applications, and future opportunities. *Front. Sens.* **2023**, *4*, 1322906. [CrossRef]
23. Choi, K.R.; Ahn, D.H.; Jung, S.Y.; Lee, Y.H.; Lee, S.Y. Microbial lysates repurposed as liquid egg substitutes. *npj Sci. Food* **2024**, *8*, 35, Correction in *npj Sci. Food* **2024**, *8*, 45. https://doi.org/10.1038/s41538-024-00281-y. [CrossRef] [PubMed]
24. Doan, V.S.; Saingam, P.; Yan, T.; Shin, S. A trace amount of surfactants enables diffusiophoretic swimming of bacteria. *ACS Nano* **2020**, *14*, 14219–14227. [CrossRef] [PubMed]
25. Serwer, P.; Hunter, B.; Wright, E.T. Cell–gel interactions of in-gel propagating bacteria. *BMC Res. Notes* **2018**, *11*, 699. [CrossRef] [PubMed]
26. Cudmore, S.; Cossart, P.; Griffiths, G.; Way, M. Actin-based motility of vaccinia virus. *Nature* **1995**, *378*, 636–638. [CrossRef] [PubMed]
27. Taylor, M.; Koyuncu, O.; Enquist, L. Subversion of the actin cytoskeleton during viral infection. *Nat. Rev. Microbiol.* **2011**, *9*, 427–439. [CrossRef] [PubMed]
28. Yoshida, A.; Uekusa, Y.; Suzuki, T.; Bauer, M.; Sakai, N.; Yamauchi, Y. Enhanced visualization of influenza A virus entry into living cells using virus-view atomic force microscopy. *Proc. Natl. Acad. Sci. USA* **2025**, *122*, e2500660122. [CrossRef] [PubMed]
29. Perrin, J. *Atoms*; D. Van Nostrand Company: New York, NY, USA, 1916; pp. 48–52.
30. Griess, G.A.; Guiseley, K.B.; Serwer, P. The relationship of agarose gel structure to the sieving of spheres during agarose gel electrophoresis. *Biophys. J.* **1993**, *65*, 1383–1393. [CrossRef] [PubMed]
31. Szermer-Olearnik, B.; Drab, M.; Mąkosa, M.; Zembala, M.; Barbasz, J.; Dąbrowska, K.; Boratyński, J. Aggregation/dispersion transitions of T4 phage triggered by environmental ion availability. *J. Nanobiotechnol.* **2017**, *15*, 32. [CrossRef] [PubMed]
32. Drab, M. Phage aggregation-dispersion by ions: Striving beyond antibacterial therapy. *Trends Biotechnol.* **2018**, *36*, 875–881. [CrossRef] [PubMed]

Disclaimer/Publisher's Note: The statements, opinions and data contained in all publications are solely those of the individual author(s) and contributor(s) and not of MDPI and/or the editor(s). MDPI and/or the editor(s) disclaim responsibility for any injury to people or property resulting from any ideas, methods, instructions or products referred to in the content.